FERMILAB-PUB-23-799-LBNF-STUDENT

Measurement of Rayleigh Scattering in Liquid Argon at Vacuum Ultraviolet Wavelengths

Larry Zhao[1]
Fermi National Accelerator Laboratory, SULI Intern

(*Electronic mail: zhao_larry@berkeley.edu.)

(Dated: 8 December 2023)

Liquid argon based detectors are limited in scintillation light analysis techniques due to inconsistent published values of fundamental constants essential for reconstructing scintillation events. This experiment measures the Rayleigh scattering length of vacuum ultraviolet light propagating in liquid argon to support liquid argon experiments by expanding the scope of scintillation signal analysis. Preliminary results are presented for the Rayleigh scattering length in a range of vacuum ultraviolet wavelengths, including the liquid argon scintillation peak wavelength. Currently, further data collection and analysis is required to reduce measurement uncertainty as well as quantify and correct for other effects such as the photon detector temperature dependence. Results will contribute to the development of new photon detector system analysis methods for liquid argon experiments.

I. INTRODUCTION

In this measurement, we aim to measure light attenuation from Rayleigh scattering in liquid argon for a range of vacuum-ultraviolet (VUV) wavelengths from 124 to 180 nm. This measurement will support the advancement of scintillation photon analysis in liquid argon time projection chambers (LArTPCs) and innovate new error reduction capabilities for neutrino experiments such as DUNE and dark matter experiments such as DarkSide.

A. Background

The Deep Underground Neutrino Experiment (DUNE)[1] primary physics objectives are to conduct precision measurements of long baseline neutrino oscillations, observe neutrinos from rare galactic supernova events, and potentially discover nucleon decays. The precision oscillation measurement aims to answer major neutrino physics questions such as the order of neutrino masses, the existence of potential CP violation in the lepton sector, and if the neutrino mixing matrix is unitary. Neutrinos produced by a supernova event creates rare opportunities to study astroparticle physics in extreme environments where neutrino-neutrino interactions may be measured. Observing nucleon decays would be a major discovery and advance beyond the standard model physics.

DUNE consists of the Long Baseline Neutrino Facility (LBNF) and a near detector at Fermilab, as well as a far detector located underground at the Homestake Mine in South Dakota. The LBNF produces a high intensity neutrino beam and the initial beam composition is measured by the near detector in support of the long baseline neutrino oscillation measurement. The far detector measures the neutrino beam spectrum after oscillations, detects potential supernova neutrinos, and searches for nucleon decays. The far detector consists of four time projection chambers (TPCs) containing 40 kilotons of liquid argon in total.

Scintillation light is a characteristic spectrum emitted by a scintillator material after excitation by ionizing radiation. Liquid argon is an excellent scintillating medium and produces a large amount of scintillation light. The nominal 500 V/cm electric field design of DUNE produces 26,000 scintillation photons per MeV of deposited energy. At lower electric fields, even more scintillation light is emitted due to more ionized electrons recombining with argon ions. Argon is also relatively transparent to its own scintillation light because light emission requires the dissociation of dimers formed by excited argon atoms, which are generally not present to reabsorb the propagating photons. The argon scintillation light spectrum features a narrow primary peak centered at 128 nm in the vacuum ultraviolet wavelength regime. Of the energy deposited by particles, $\sim$60% produces scintillation light and $\sim$40% produces ionized drift electrons.

In TPCs, a charged particle ionizes the argon atoms, an applied electric field causes the ionized charge to drift towards the anode over a time span of milliseconds, and readout wires or planes record the detected charge pattern in space in two dimensions while the drift time reconstructs the third dimension. Scintillation light does not provide fine spatial resolution of signals, but is still critical to measuring the third spatial dimension. Reconstructing the absolute position where particles pass through the volume requires knowing the time difference in arrival between scintillation light (time from emission to detection of order nanoseconds) and ionization drift electrons (velocity of 1 mm/μs). This is the only measurement of the absolute time for reconstruction of absolute position in non-beam events such as supernova neutrinos and nucleon decays. The absolute position is key to defining fiducial volumes to exclude background signals and correct for the attenuation of charge signals in flight.

B. Motivation

Though the scintillation photon detector system primarily functions to reconstruct position information, it can also advance DUNE's physics goals further by enabling a second calorimetric measurement of the total event energy. The addition of an alternative energy measurement improves analysis by increasing energy resolution (since the photon and charge energy measurements resolution have different limitations), as well as provide a cross check of the energy measurement, allowing for reductions in the systematic uncertainty. The improved analytical sensitivity can contribute to DUNE's physics objectives, and gains in systematic uncertainty reduction are particularly important for precision measurements of small oscillation effects. However, developing this new application of the photon detector system requires measurements of fundamental constants to accurately reconstruct the deposited energy from scintillation photons. Critically, there is no consensus on the total attenuation due to the Rayleigh scattering length of scintillation photons propagating in liquid argon.

The total attenuation length L is related to absorption length L_A and scattering length L_S by

$$\frac{1}{L} = \frac{1}{L_A} + \frac{1}{L_S} \tag{1}$$

where we expect the total attenuation length to be primarily dominated by Rayleigh scattering. For measurements at different wavelengths and liquid argon depths, the Rayleigh scattering ratio R at 90°is

$$R = \frac{I}{I_0}\frac{r^2}{V} \propto \frac{1}{\lambda^4} \tag{2}$$

where I is the scattered intensity, I_0 is the incident intensity, r is distance from the scattering center to the detector, and V is the scattering volume.

Experiments such as Ishida et al[2] measured the attenuation length of $\lambda = 128$ nm photons in liquid argon to be 66 ± 3 cm. Neumeier et al[3][4] then measured an attenuation length of 1.63 m, and subsequently established a lower bound of 1.1 m. Later, M. Babicz et al[5][6] derived a Rayleigh scattering length of 91.0 ± 2.3 cm and then 99.1 ± 2.3 cm from measurements of $\lambda = 128$ nm photon velocity in liquid argon.

In addition, Neumeier et al[3] found that the VUV photon attenuation length in liquid argon is not described by a single universal value due to wavelength dependent emission and absorption. They also reported absorption and emission line effects due to the presence of oxygen, water, and xenon contamination. Other impurities such as nitrogen also impact liquid argon measurements, as reported by the WArP collaboration[7] and Jones et al[8].

Calculations by Seidel, Lanou, and Yao[9] yielded a 90 cm scattering length, while Grace et al[10] calculated a 55 ± 5 cm scattering length. The disparity in the scattering length calculation is attributed to the required extrapolation of properties of liquid argon from longer wavelengths and sometimes from gas to liquid. The factor of three variation in previous Rayleigh scattering length experiments and calculations requires further investigation to determine the true scattering length.

II. EXPERIMENTAL DESIGN

A. Experimental Setup

The Noble Liquid Test Facility (NLTF) in the Proton Assembly Building (PAB) at Fermilab offers extensive research and development infrastructure for optical tests in ultra pure liquid argon. The scintillation photon attenuation measurement in liquid argon is conducted using the TallBo cryostat (Fig. 1) situated at the NLTF.

A deuterium lamp installed above the cryostat produces a light spectrum, which includes the ultraviolet wavelength range of interest. The deuterium lamp spectrum is reduced to a narrow wavelength band by a monochromator. The resulting light is collimated by a collimator so the photons travel in parallel, thus reducing beam divergence and refracted light inside the cryostat. Finally, the monochromatic photon beam enters the cryostat perpendicular to the liquid argon surface below. Reflection suppressors line the bottom and sides of the cryostat to prevent detection of reflected photons. Gaseous argon purges the monochromator system to remove contaminant gases and prevent buildup of absorptive materials on the deuterium lamp window. The cryostat also uses a condenser system to control the pressure of the volume of gaseous argon above the liquid argon.

Silicon photomultiplier (SiPM) photodetectors measure the photon signals incident upon its active area. Ten Hamamatsu VUV4 S13370-6050CN 6×6 mm^2 SiPMs (numbered channels 0 to 9) are installed at strategic positions on the bottom (channel 0 and 1) and side (channel 2 to 9, in order from bottom to top) of the cryostat to collect scattered photons. This SiPM model is sensitive to photons down to $\lambda = 120$ nm[11], removing the requirement of wavelength shifting coatings used in experiments with previous generations of SiPMs. A SiPM Signal Processor (SSP) applies the SiPM bias voltages, sets trigger thresholds for data collection, converts analog SiPM

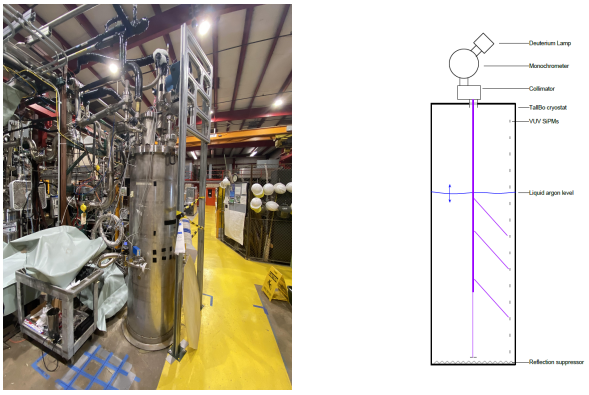

(a) TallBo Cryostat (b) Cryostat Diagram

FIG. 1: TallBo Cryostat

signals to digital values, and analyzes the data. LBNEWare software interfaces with the SSP and is used for applications such as inputting the SiPM bias voltage and signal trigger threshold settings, setting values related to the signal readout and analysis parameters, as well as displaying recorded waveform signals.

The TallBo cryostat possesses a calibrated level meter to determine the liquid argon depth. Gas analyzers for nitrogen, oxygen, and water are used to confirm the liquid argon purity inside the cryostat. Other sensors monitor the temperature and vacuum pressure inside the cryostat.

B. Procedure

First, we fill the cryostat with liquid argon to the maximum fill level and submerge the SiPMs. The SiPM detector response depends on the temperature, thus only SiPMs submerged in liquid argon are used for characterization of signal behavior. Of the installed SiPMs, channels number 1, 2, 4, 5, and 6 are operated for the measurement. SiPM signal waveforms (Fig. 2) exceeding the trigger threshold are processed and recorded in output files. The SiPM dark signal rate at liquid argon cryogenic temperatures is standardized to $\sim$100 Hz for each SiPM by setting the trigger thresholds to the same values and tuning the applied bias voltages. Current inputs are set at a value of 20 for the leading edge discriminator threshold to reduce noise signal triggers, and a range from 43.80 V to 44.22 V for the SiPM bias voltages.

Initial data collection procedures used Python commands to alternate between shutter closed and shutter open states in 1 second intervals. For each shutter open period, we also incremented the monochromator to a new wavelength. However, data collection using this procedure resulted in multiple unforeseen issues. First, the Arduino device generating regular electronic timing pulses to sync the computer and SSP timestamps did not interact correctly with the SSP in addition to causing electrical grounding problems. Attempted solutions, such as using a TTL/NIM converter to rectify the Arduino signal, also failed to reliably synchronize the Arduino and SSP pulses. Second, operating the monochromator motor

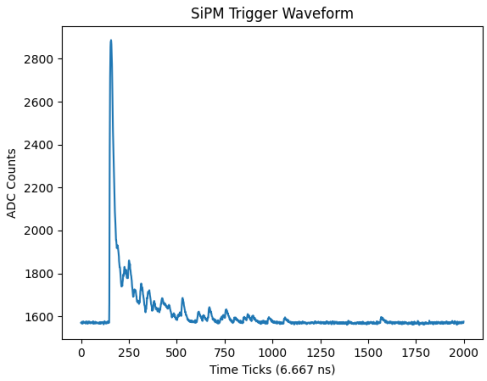

FIG. 2: Example SiPM Signal Waveform

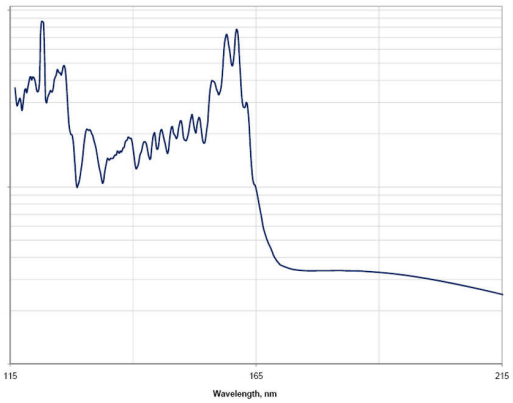

FIG. 3: McPherson Deuterium Lamp Spectrum[12]

power supply simultaneously to the SiPMs caused anomalous responses in the SiPM waveforms, likely due to electronic grounding issues. As a result, later measurement runs exclude operation of the Arduino, SSP sync, and monochromator motor during data collection. Third, the LBNEWare software data collection is limited to 50,000 triggers per run, so it is not possible to collect data for the entire wavelength range in one run. Furthermore, data transfer via USB cable from the SSP to the computer saturates under high trigger rates, which necessitated disabling the recording of waveform data and only saving the SSP calculated values.

The results from testing initial procedures informed the methods developed for the data collection procedures. For each liquid level in the first data collection run, 50,000 SiPM dark signals are measured to quantify the background due to dark counts, cosmic ray scintillations (e.g. cosmic muons), and radioactive decays (e.g. argon isotopes like ^{38}Ar). The monochromator is then set to the desired single wavelength, the shutter is opened to measure photons, and the SSP records 50,000 triggers. Next, we repeat the shutter open measurement with the monochromator set to the next wavelength. We scan the wavelength range from 124 nm to 180 nm, encompassing both the liquid argon and liquid xenon scintillation wavelengths of 128 and 175 nm, respectively. We note that the data rate saturates at certain wavelengths (e.g. 160 nm) due to intense peaks in the deuterium lamp spectrum (Fig. 3). The dark signals are then measured a second time to determine the background rate variation across the run. The liquid level is lowered, and the wavelength scan measurement procedure is repeated for each liquid level.

Analysis of the first run data prompted investigation into sources contributing to inexplicable effects. Further measurements from the second data collection run found that the deuterium lamp intensity varies significantly over time, and can take over 8 hours to reach equilibrium using the Run 1 procedures (Fig. 4). The deuterium lamp intensity is expected to stabilize after 30 minutes, but the gaseous flush setting for the monochromator resulted in changing levels of impurities. These impurities absorb VUV light and caused varying light intensity over time inside the cryostat. The second data collection run attempted to quantify the deuterium lamp and

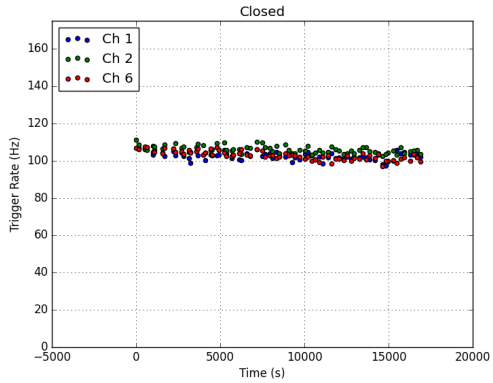

(a) Background Rate vs Time

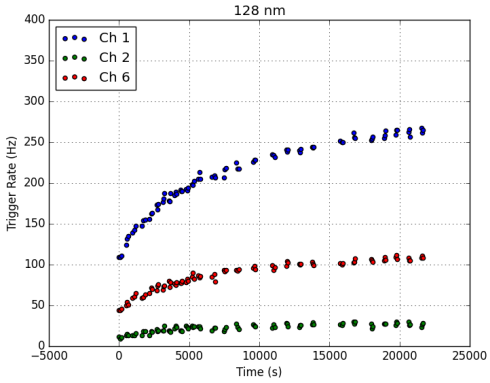

(b) 128 nm Rate (Background Subtraction) vs Time

FIG. 4: Run 2, 60in Liquid Argon Depth

monochromator flush warm up curve in order to apply data analysis corrections. However, differing flush rates resulted in different warm-up curve fit parameters and meant the corrections could not be applied. The light intensity instability issue was solved by changing the gaseous flush setup to allow for overnight use, which removed steps for turning on the gaseous flush and deuterium lamp at the beginning of each day that resulted in inconsistent impurity levels and light intensity.

For the third data collection run, we confirm the light intensity stability by measuring shutter closed and 128 nm light triggers over time. This step also functions to compare the change in background signal rates and lamp intensity overnight between periods of data collection. Despite variation overnight in background signal rates, the background subtracted light detection rates remained stable. Further, a hardware incident caused by a rupture disk failure on the liquid nitrogen storage tank resulted in the tank open to atmosphere with no positive pressure inside. The liquid nitrogen system is instrumental in the condenser operation and controlling the argon gas pressure inside the cryostat. The loss of liquid nitrogen pressure control meant the cryostat was opened to atmosphere. Further tests indicated the varying pressure levels during the data collection period following the issue do not have significant effects on VUV light transmission inside the cryostat.

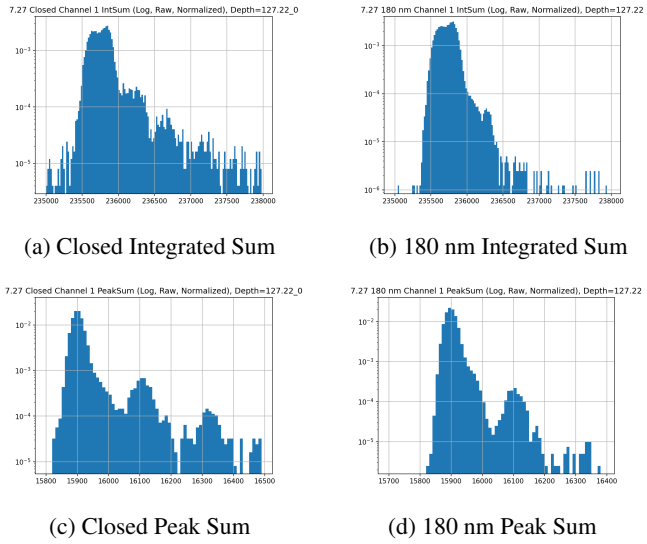

(a) Closed Integrated Sum

(b) 180 nm Integrated Sum

(c) Closed Peak Sum

(d) 180 nm Peak Sum

FIG. 5: Run 1, SiPM 1 Waveform Analysis Histograms

III. ANALYSIS

Initial data analysis studies supported optimization of data collection settings as well as analysis techniques. Investigating the waveform and SSP calculated values for integrated sum (sum of a tunable number of waveform values in the peak) and peak sum (sum of a tunable number of waveform values in a subset of the peak) with no background subtraction indicates that a single trigger event generally corresponds to one incident photon (Fig. 5). The majority of integrated sum and peak sum values are distributed around a central value. A smaller number of events are distributed around a higher value (below the high energy background signal peaks), consistent with cross-talk between SiPM pixels. As a result, we expect the number of low energy trigger events to be equal to the number of light source photons detected.

To account for differences in time length between runs, we use background subtracted trigger rate ((Trigger Number − Background Number)/Run Time Length) as the primary

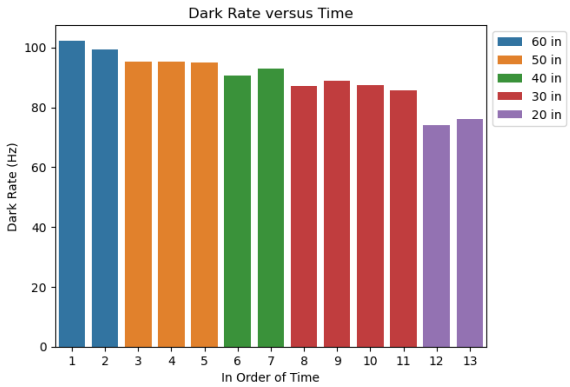

FIG. 6: Dark Rate vs Liquid Level

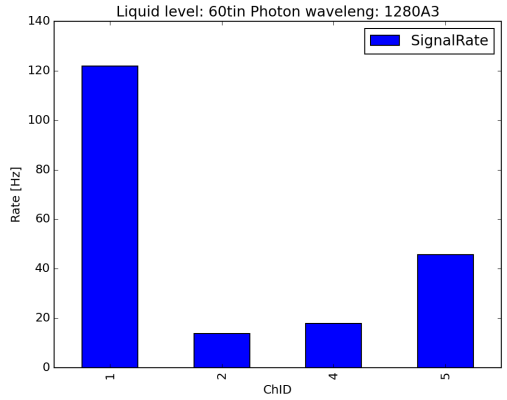

FIG. 7: Background Subtracted Rates (127.22 cm depth)

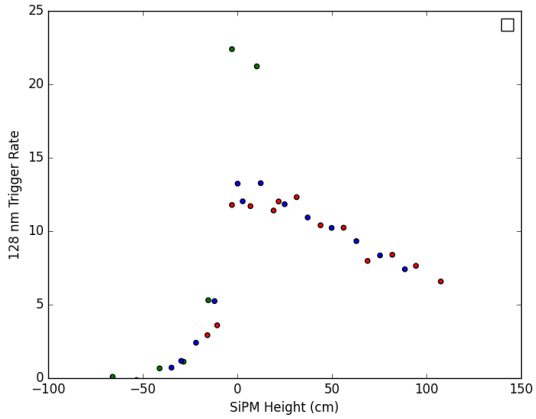

FIG. 9: SiPM Rate vs SiPM Liquid Argon Depth, 128 nm (Channel 2-Red, Channel 4-Blue, Channel 5-Green)

analysis metric. The background rates display small variations over time, but more significantly depend on liquid level (Fig. 6). Lower background rates at lower liquid levels are explained by less scintillation signal rates in the smaller volume from cosmic rays (e.g. atmospheric muons) and radioactive decays of argon isotopes (e.g. ^{38}Ar).

Confirmation of measuring exclusively Rayleigh scattering effects relies on several tests. First, we expect the largest number of scattered photon signals on the SiPMs close to the liquid argon surface because the light intensity is greatest at the beam point of entry. As a result, more light is available for scattering near the liquid surface compared to at greater depths. (Fig. 7) corroborates the expected trend, but does not match expected numerical proportions from simulation results. As a result, we compare signals in a single channel at different liquid levels, instead of comparing signals between different channels at a single liquid level.

A second test is to measure the liquid argon triplet lifetime,

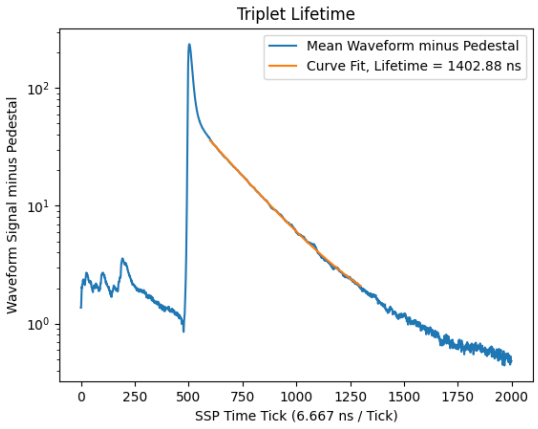

FIG. 8: SiPM Rate versus SiPM Distance to Liquid Argon Surface, 128 nm (Channel 2-Red, Channel 4-Blue, Channel 5-Green)

which gives insight into potential attenuation from impurities. The triplet lifetime is measured by setting a high trigger threshold and taking data with the shutter closed. As a result, the collected data is largely high energy scintillation signals from cosmic rays and radioactive decays. Since the data acquisition system records the data for each waveform with the same peak position, we can take the mean of each point in the waveform across all triggers to generate a curve of the signal decay. Applying a curve fit results in a triplet lifetime value for comparison to the known triplet lifetime of liquid argon is 1.3 μs. We measured a liquid argon triplet lifetime of 1.4 μs for Channel 1, (Fig. 8), indicating high purity liquid argon in the cryostat.

Further plots of signal rate versus SiPM depth (Fig. 9) show that Channels 2 and 4 are consistent in gain, but Channel 5 is not. This effect is likely due to the presence of a temperature gradient in liquid argon concentrated near the surface level, therefore resulting in different Channel 5 SiPM temperature when determining bias voltages and a different SiPM response. To ensure accurate data from Channel 5 and 6 as well as the other channels at lower liquid levels, further measurements to understand and correct for the temperature gradient in the liquid argon are needed.

The total photon rate across the wavelength range demonstrates reasonable behavior (Fig. 10) when accounting for the deuterium emission spectrum (Fig. 3), the SiPM detection efficiency[11], and the relation given in (Eq. 2). Investigating integrated sum and peak sum indicates the multi photon (greater than second lowest peak or 3PE) event rate is roughly constant (Tab. I), indicating those triggers are most likely a constant background from cosmic rays and radioactive isotope decays. As a result, we expect the number of trigger events in the first two Integrated Sum and Peak Sum peaks (Fig. 5) to be equal to the number of photons detected. This result informs further analysis methods to identify background signal sources and improve analysis of trigger rates.

Calculations of errors depend on the fact the measurement

records the maximum 50,000 triggers for each file (run all SiPMs at one wavelength, one liquid depth). The trigger rate errors are then calculated as follows for signal S, background B, and photon rate $R = S - B$:

$$\frac{\delta S}{S} = \frac{\delta B}{B} = \frac{\delta N}{N} = \frac{1}{\sqrt{50000}} \simeq 0.5\% \tag{3}$$

$$\delta(S-B)^2 = \delta S^2 + \delta B^2 = S^2\left(\frac{\delta S}{S}\right)^2 + B^2\left(\frac{\delta B}{B}\right)^2 \tag{4}$$

$$\frac{\delta R}{R} = \left(\frac{\delta N}{N}\right)\frac{\sqrt{S^2+B^2}}{S-B} \tag{5}$$

For a signal rate of 120 Hz and background rate of 80 Hz, the background subtracted rate measurement error is approximately 1.8%. This factors into the error bars for the trigger rate vs depth curve fit parameter and parameter errors.

IV. CONCLUSIONS

Preliminary Run 3 measurements are presented for Rayleigh scattering length at wavelengths from 124 to 180 nm. However, the data and analysis produces features that require further exploration. In addition, the analysis curve fitting still results in significant fit parameter uncertainties due to uncertainties in the background subtracted rates. The current measured Rayleigh scattering length for the 128 nm liquid argon scintillation peak is 125.7 ± 22.37 cm.

A. Future Objectives

Further investigations into analysis selections to identify background signals, find understanding unexpected patterns in background subtracted photon rates, and explaining other unknown phenomena are required. More data runs will take place in the Fall of 2023 to continue investigating solutions and conclude measurement results.

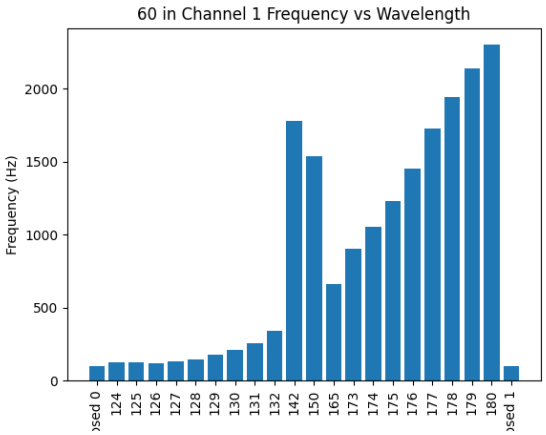

FIG. 10: Rate versus Wavelength (127.22 cm)

Acknowledgements: Dr. Alex Himmel and Dr. Wei Mu are instrumental to work presented in this paper. Dr. Alex Himmel conceived and designed the experiment in addition to securing funding for equipment and personnel to conduct the measurement. Dr. Alex Himmel and Dr. Wei Mu commissioned the experiment and are also worked on optimizing hardware and software setups, collecting data, and developing analysis methods. Dr. Wei Mu contributed Figures 2, 5, 7, and 9 in this paper.

c. This manuscript has been authored by Fermi Research Alliance, LLC under Contract No. DE-AC02-07CH11359 with the U.S. Department of Energy, Office of Science, Office of High Energy Physics.

d. This work was supported in part by the U.S. Department of Energy, Office of Science, Office of Workforce Development for Teachers and Scientists (WDTS) under the Science Undergraduate Laboratory Internships Program (SULI).

[1] A. I. Himmel, "Seeing Neutrinos: The Physics Potential of Photon Signals in DUNE,".
[2] N. Ishida et al., "Attenuation length measurements of scintillation light in liquid rare gases and their mixtures using an improved reflection suppresser," Nucl. Instr. and Meth. in Phys. Res. A **384**, 380–386 (1997).
[3] A. Neumeier et al., "Attenuation of vacuum ultraviolet light in liquid argon," Eur Phys. J. C **72** (2012).
[4] A. Neumeier et al., "Attenuation of vacuum ultraviolet light in pure and xenon-doped liquid argon - an approach to an assignment of the near-infrared emission from the mixture," EPL **111** (2015).
[5] M. Babicz et al., "Experimental study of the propagation of scintillation light in liquid argon," Nuclear Inst. and Methods in Physics Research, A **936**, 178–179 (2019).
[6] M. Babicz et al., "A measurement of the group velocity of scintillation light in liquid argon," JINST **15** (2020).
[7] R. Acciarri et al., "Effects of nitrogen contamination in liquid argon," JINST **5** (2010).
[8] B.J.P. Jones et al., "A measurement of the absorption of liquid argon scintillation light by dissolved nitrogen at the part-per-million level," JINST **8** (2013).
[9] G.M. Seidel, R.E. Lanou, W. Yao, "Rayleigh scattering in rare-gas liquids," Nuclear Instruments and Methods in Physics Research Section A **489**, 189–194 (2002).
[10] E. Grace et al, "Index of refraction, rayleigh scattering length, and sellmeier coefficients in solid and liquid argon and xenon," Nuclear Inst. and Methods in Physics Research, A **867**, 204–208 (2017).
[11] *VUV-MPPC 4th generation (VUV4) Product Flyer*, Hamamatsu (2017).
[12] *Deuterium Source with Magnesium Fluoride Window*, McPherson (2017).

Appendix A: Appendixes

TABLE I: Total and Third Peak Sum Peak Trigger Rate for Channel 1 and Channel 2

Wavelength	Ch 1 Rate 3PE	Ch 1 Total Rate	Ch 2 Rate 3PE	Ch 2 Total Rate
Closed	1.114702098	102.3247707	0.7404225613	100.5428746
124	1.056804038	125.4932594	0.8170249709	103.5579151
125	0.9924281097	122.3936118	0.8255596665	104.4420804
126	1.056945719	120.9897121	0.7512176188	102.445119
127	1.069047503	129.7556406	0.6859721475	103.6174292
128	1.080057264	146.0730079	0.862150974	105.5708605
129	0.9905293452	174.7768394	0.846077149	109.0923622
130	1.077132777	209.2245382	0.7596620637	111.6589851
131	1.251333603	256.4475502	0.8595018687	116.3866648
132	0.8422378213	339.6775213	0.9475175489	124.5007979
142	1.142222238	1777.959089	0.9017543985	322.5876068
150	0.3041595671	1540.203216	0.851646788	421.4434962
165	1.069427662	662.8983661	0.8807051332	123.8858554
173	1.168730067	904.3373543	0.9349840538	126.9240853
174	1.147285162	1057.149733	0.7648567748	135.114891
175	1.159506982	1232.191506	1.026991899	141.0954354
176	1.597352275	1453.400409	0.8367083346	147.5268923
177	1.502471773	1728.107681	0.6628551941	155.3732575
178	1.270036225	1944.327766	1.074646037	162.6134844
179	1.761626362	2142.671482	0.5338261702	174.1340967
180	1.252850075	2301.884222	0.5694773068	178.5311357
Closed	1.125053412	99.22346065	0.7656613499	99.02032601